Structural, Optical, Magnetic and Photon Attenuation of Novel Potassium Lead Borate Glasses Doped with MnO

A. S. Abouhaswa (aliabohaswa@hotmail.com)
Menoufia University

Y. S. Rammah
Ural Federal University

Research Article

Keywords: Mn-glasses, FTIR, Optical, Magnetic, Phy-X/PSD, Gamma-ray, Protection materials

Posted Date: December 28th, 2021

DOI: https://doi.org/10.21203/rs.3.rs-1193099/v1

Version of Record: A version of this preprint was published at Journal of Inorganic and Organometallic Polymers and Materials on March 10th, 2022. See the published version at https://doi.org/10.1007/s10904-022-02272-6.

Structural, optical, magnetic and photon attenuation of novel potassium lead borate glasses doped with MnO

A.S. Abouhaswa[1,2], Y.S. Rammah[1]

[1]Department of Physics, Faculty of Science, Menoufia University, Shebin El-Koom 32511, Menoufia, Egypt

[2]Ural Federal University, Yekaterinburg, Sverdlovskaya oblast, 620002, Russia

Abstract

Potassium lead borate glasses doped with MnO ($40B_2O_3$+40PbO+(20-x)K_2O+xMnO: x= 0-5 mol%) have been prepared via standard melting quenching process. The impact of MnO on the structure, optical, magnetic and gamma-ray protection properties of pottisium lead borate glasses have been examined. The density was increased from 4.83±0.01 to 5.23±0.01 g/cm^3 as MnO content increased. The obtained direct optical gap (E_g) values were 2.84, 2.59, 2.41, 2.19, 1.95, and 1.84 eV for the Mn-x (x=0, 1, 2, 3, 4, and 5) glass samples, respectively. FTIR spectra demonstrated that as the MnO concentration increases in the glass network the intensity and width of the IR bands were increased. The magnetic measurement revealed that the magnetic situation (M_s) was decreased while the magnetic coercivity (H_c) was increased with increasing MnO substitution ratio. The linear attenuation coefficient of the $\mu_{Mn-glass}$ follows the order: $\mu_{Mn\text{-}0} < \mu_{Mn\text{-}1} < \mu_{Mn\text{-}2} < \mu_{Mn\text{-}3} < \mu_{Mn\text{-}4} < \mu_{Mn\text{-}5}$. Half value layer (HVL) rises as μ decreases and vice versa. The range of the HVL is 0.002 – 3.378, 0.002 – 3.334, 0.002 – 3.291, 0.002 – 3.248, 0.002 – 3.176, and 0.002 – 3.106 cm for Mn-x (x=0, 1, 2, 3, 4, and5). The trend of Z_{eff} variation is related to that of both linear and mass attenuation coefficients (μ and μ_m). The produced Mn-glasses can be employed in a variety of optical, magnetic and radiation protective applications.

Keywords: Mn-glasses; FTIR; Optical; Magnetic; Phy-X/PSD . Gamma-ray; Protection materials

Corresponding author: aliabohaswa@hotmail.com (A. S. abouhaswa)

Introduction

Because of their wide range of applications, glasses offer a distinct advantage over other types of materials. Optical fibres, solid state lasers, water treatment, and optical filters considered as examples of technological and biological applications of glasses [1-9]. A growing number of studies have looked into the subject of glasses. Because of the distinctive physical, chemical, electrical, magnetic, and optical characteristics of boron-based glasses, the number of research and investigations has increased dramatically. These glasses have a significant glass-forming nature and low softening and melting temperatures. Furthermore, boron-based glasses are known to have a variety of truly amazing, including high electrical conductivity, high thermal expansion coefficients, low thermal conductivity, and low dispersion [7]. All these properties make boron glasses have more advantageous compared to further conventional glass formers for instance phosphate, germanate and silicate [6-9].

The effects of manganese (Mn) ions on the physical and structural features of diverse glass systems such as borate, tellurite, and phosphate have been studied by a number of researchers [10-12]. Manganese has more stable valence states such as Mn^{2+}, Mn^{3+}, and Mn^{4+} [13]. Only Mn-containing glasses had the second and third oxidation states. Mn^{2+} ions in the glass network have a significant influence on optical characteristics [14].

Glasses contain heavy metal oxide (HMO) such as PbO, Bi_2O_3, and others have more attention from several technologists, researchers, and investigators due to their interesting structural, physical and physiochemical characteristics like as substantial improvements in their linear/nonlinear optical features and radiation protection application [15-20].

The aim of the present work is to investigate the impact MnO on the structure, optical, magnetic properties, and gamma-ray protection parameters of the prepared potassium lead borate glasses doped with MnO.

2. Experimental technique, measurements, and calculations

2.1 Mn-glasses preparation

Via using the standard melting quenching process, six glass samples with compositions $40B_2O_3$+40PbO+(20-x)K_2O+xMnO have been synthesized. Boron oxide (B_2O_3) 99.99%, lead oxide (PbO) 99.99%, potassium oxide (K_2O) 99.998%, Manganese oxide (MnO) 99.99% have been mixed carefully. Subsequently, the mixed powder pre-heated for 60 minutes at 300°C. The resulting combinations were melted at 1000 - 1080 °C for 30 minutes. Then poured onto a stainless-steel mold to manufacture glass samples in discs form. After quenching, the glass samples are typically moved to a muffle furnace set to 300°C for annealing.

2.2 Measurements and calculation

In the current study, Archimedes' technique (Equation 1) was used to determine the densities of Mn-glasses with toluene as an immersion liquid with density ($\rho_{toluene}$). Considering W_b is the weight of glasses in toluene liquid, and W_a is the weight of the glasses in air, the glass density can be given by:

$$\rho_{glass} = \frac{W_a}{W_a - W_b}\rho_{tolune} \quad (1)$$

The infrared absorption spectra of the produced Mn-glasses were measured at room temperature in the range 4000– 400 cm^{-1} via an infrared spectrometer type Jasco FTIR-300E (Japan).

In order to evaluate the optical data of the polished prepared Mn-glass samples, Cary 5000 UV–Vis-NIR double beam spectrophotometer was used.

Using the vibrating sample magnetometer (VSM), the magnetic hysteresis characteristics of the prepared glasses in magnetic fields with intensities up to 20 kOe at room temperature.

All gamma radiation shielding parameters presented in the current work were evaluated by Phy-X/PSD software [21] as:

Mass attenuation coefficients (MAC = μ/ρ)

$$\frac{\mu}{\rho} = \mu_m = \sum_i W_i \left(\frac{\mu}{\rho}\right)_i \quad (3)$$

Linear attenuation coefficient (LAC = μ= μ_m x ρ) (4)

μ and μ/ρ were used to calculate the half value layer (HVL) and effective atomic number (Z_{eff}) as follows:

$$HVL = T_{1/2} = \frac{0.693}{\mu} \quad (5)$$

$$Z_{eff} = \frac{\sum_i f_i A_i \left(\frac{\mu}{\rho}\right)_i}{\sum_j \frac{A_j}{Z_j} \left(\frac{\mu}{\rho}\right)_j} \quad (6)$$

3. Results and discussion

3.1 Density, FTIR analysis, and optical properties

Figure 1 illustrates densities of the prepared Mn-glass samples as a function of MnO content in glass compositions. Densities were 4.83, 4.89, 4.95, 5.01, 5.12, and 5.23 g.cm^{-3} for Mn-0, Mn-1, Mn-2, Mn-3, Mn-4, and Mn-5 glasses, respectively. The difference in density between MnO (5.37 g.cm^{-3}) and K_2O (2.35 g.cm^{-3}) causes an increase in the density of glass samples as MnO content increases.

The FTIR spectra of the fabricated glass samples with the composition $40B_2O_3$+40PbO+(20-x)K_2O+xMnO (x= 0, 1, 3, and 5 mol%) were recorded at room temperature in the spectral region of 400–4000 cm^{-1} and presented in Figure 2. The vibrational modes of the glass samples under investigation may be divided into three infrared spectral ranges [22-24]. Asymmetrical stretching vibrational modes occurring in the B—O band of the trigonal [BO_3] units can be attributed to the first region in the range of 1200–1800 cm^{-1}. The stretching vibrations occurring in the B—O band of the

tetrahedral [BO_4] units are described in the second area, which ranges 800–1200 cm^{-1}. The third band is seen between 400 and 800 cm^{-1} is ascribed to the bending vibrations of different borate arrangements and the vibration of metal cations like Pb^{2+}, K^{1+} and Mn^{2+} across the glass network. Table 2 depicts the vibrational groups in IR spectra in the spectral region of 400–4000 cm^{-1} [25, 26]. Many peaks have been resolved for all of the samples using the deconvoluted spectra, as shown in Figure 3 (a - d). The peak position (x_c), amplitude (A), and full width at half maximum (W) of the peaks produced from the deconvolution technique are shown in Table 3. The deconvoluted spectra of the different samples demonstrate that as the MnO_2 concentration increases in the glass network the intensity and width of the IR bands were increased. This is attributed to a higher degree of disorder when more Mn^{2+} ions access the network and serve as structural modifiers. This results in a significant increase in the amount of non-bridging oxygen atoms, which has an impact on the structural stability of the glass system [27]. On the basis of the following discussion, it can be assumed that the addition of MnO in place of K_2O resulted in structural modifications.

The absorbance spectra of the prepared Mn-glasses are shown in Figure 4. It was clear that the optical absorption edge is shifted to higher wavelength with the increase of MnO content in the prepared glasses. According to the absorption spectra, the optical band gap (E_g) values are evaluated in the context of a Tauc's relation between absorption coefficient $\alpha(\nu)$ and the photon energy ($E = h\nu$) as [28],

$$(\alpha h\nu)=K(\hbar\nu - E_g)^s \qquad (7)$$

where K is a constant and s may has the following values 2, 3, 1/2 and 1/3 depending on the type of electronic transitions [29]. Herein, we used s = 1/2 indicating the direct electronic transition. Because of the predominant transitions in glasses are direct or indirect which acquire the absorption of photons near the E_g [30]. Variation of $(\alpha h\nu)^2$ with $(h\nu)$ of the prepared Mn-glasses is shown in Figure 5. By extrapolating the linear section using straight line until meets the $h\nu$-axis at values equal the E_g. The evaluated E_g values

were 2.84, 2.59, 2.41, 2.19, 1.95, and 1.84 eV for the Mn-0, Mn-1, Mn-2, Mn-3, Mn-4, and Mn5 glass samples, respectively. These values are listed in Table 4, it is obvious from these values that a further doping of MnO results in a reduction in E_g values. This reduction in E_g values is linked with the increased content of non-bridging oxygens (NBO) within the glass matrix [31,32].

Urbach's empirical formula is given by:

$$\alpha = \alpha_0 exp\left(\frac{h\nu}{E_U}\right) \quad \text{and} \tag{8}$$

$$ln\alpha = ln\alpha_0 + \left(\frac{h\nu}{E_U}\right) \tag{9}$$

As a result, the slope of the straight line obtained by plotting ln(α) versus (hν) gives the Urbach's energy (E_U). The variation of (lnα) with (hν) of the prepared Mn-glasses is plotted in Figure 6. Values of Urbach's energies were evaluated and listed in Table 4. The E_U values were increased with the increasing of MnO content in the prepared Mn-glasses. This result revealed that with increasing MnO concentration in the prepared glasses, there was less stability in glass samples with more imperfections and increase disorder in the produced glass samples.

3.2 Magnetic properties:

Figure 7 shows the magnetization of prepared glass samples doped with MnO as a function of magnetic field. It was detected that undoped glass and doped glass samples with MnO exhibited a soft ferromagnetic behavior. Table 4 represents the values of saturation magnetization (M_s) and coercivity field (H_c) which estimated from the hystresis loop curve.

As well as the magnetic moment per formula unit in Bohr magnetons (μ_B) was calculated by using the following relation (10) and listed in Table 4:

$$\mu_B = \frac{M \times M_s}{5585} \tag{10}$$

where M is the molecular weight of the composition and M_s is the saturation magnetization (emu g^{-1}).

At the beginning of the MnO substitution there was a rapid decrease in saturation magnetization (M_s) and magnetic moment until Mn-2 and after that there is some improvement in the (M_s) and (μ_B), but still the sample Mn-0 has the best in saturation magnetization and magnetic moment. On the contrary, at the beginning of the replacement, the coercivity field (H_c) was improved until Mn-2, and then this improvement was decreased, but it is still better than Mn-0.

The decreasing of saturation magnetization (M_s) and magnetic moment (μ_B) with increasing MnO substitution ratios might be attributed to an increase in anti-ferromagnetic phase with a smaller ratio of ferromagnetic-like phase.

3.3 Mn-glasses as gamma-ray protection materials

Phy-X/PSD software [21] was used to evaluate the gamma radiation protection parameters. Figure 8 depicts the energy response of the (LAC=μ) of the prepared Mn-glasses. From Figure 8, it was seen that μ reduces smoothly with 0.10 ≤ photon energy (E) ≤ 8 MeV. Then, the values of μ slightly increased at 10 MeV. This trend demonstrates the reduction and increase in the photon interaction cross-sections of the Mn-glasses with respect to photon energy. Typically, within the investigated energy spectrum:

$$\mu_{material} = \mu_{PE} + \mu_{CS} + \mu_{PP} \quad (10)$$

where, μ_{PE} = the linear attenuation due to photoelectric (PE), μ_{CS} = the linear attenuation coefficient due to Compton scattering (CS), and μ_{PP} = the linear attenuation coefficient due to pair production (PP) absorption processes, respectively. The contribution of eah of these absorption processes at different energies gives the general behaviour of μ. According to energy, $\mu_{PE} \propto E^{-3}$, $\mu_{CS} \propto E^{-1}$, and $\mu_{PP} \propto E^{1}$. Consequently, the energy spectrum of the μ can be divided into three regions where each of the μ_i dominates

photon interactions. The μ_{PE} dictates the energy response of μ at 0.10 ≤ photon energy ≤ 0.5 MeV, the μ_{CS} dicates the energy response of μ at 0.5 < photon energy ≤ 8 MeV, while the μ_{PP} dicates the energy response of μ at 0.8 < photon energy ≤ 10 MeV. Thus the rapid decay in the value of μ in the low energy range is due to $\mu_{PE} \propto E^{-3}$, while the slight increase in the μ is as a result of the energy dependence of μ_{PP}. Results of the $\mu_{Mn-glass}$ follows the order: $\mu_{Mn\text{-}0} < \mu_{Mn\text{-}1} < \mu_{Mn\text{-}2} < \mu_{Mn\text{-}3} < \mu_{Mn\text{-}4} < \mu_{Mn\text{-}5}$. Generally, $\mu \propto \rho$, hence, the observed trend of μ can be attributed to the increase in the mass density (ρ) of the glasses as MnO content increases relative to K_2O. The range of μ for Mn-0, Mn-1, Mn-2, Mn-3, Mn-4, and Mn-5 is 0.205 – 344.419, 0.208 – 349.585, 0.211 – 354.776, 0.213 – 359.992, 0.218 – 368.835, and 0.223 – 377.722 cm^{-1}, correspondingly.

The (μ_m) of the prepared Mn-glasses is shown in Figure 9. The behavior in the energy response of μ_m is similar with that of μ due to $\mu_m \propto \mu$. Furthermore, the energy dependence of $(\mu_m)_{PE}$, $(\mu_m)_{CS}$, and $(\mu_m)_{PP}$ at each energy prescribe the overall energy response of μ_m of the glasses. Thus the trend of μ_m at each energy is such that $(\mu_m)_{Mn\text{-}0} < (\mu_m)_{Mn\text{-}1} < (\mu_m)_{Mn\text{-}2} < (\mu_m)_{Mn\text{-}3} < (\mu_m)_{Mn\text{-}4} < (\mu_m)_{Mn\text{-}5}$.

Another useful radiation shielding parameter is the HVL used to describe the relative photon shielding power of a material. HVL is the required thickness of the glass to reduce incident photon exposure to 50%. Figure 10 demonstrates the variation of HVL with the photon energy and MnO concentration in the prepared Mn-glasses. Quantitatively and qualitatively, the variation in the values of HVL is consistence with the inverse of μ. For energies where photon interaction probability decreases, HVL rises and vice versa. Hence, HVL rises as μ decreases and vice versa. The range of the HVL is 0.002 – 3.378, 0.002 – 3.334, 0.002 – 3.291, 0.002 – 3.248, 0.002 – 3.176, and 0.002 – 3.106 cm for Mn-0, Mn-1, Mn-2, Mn-3, Mn-4, and Mn-5, respectively. Clearly, the gradual replacement of K_2O with MnO improved the photon absorbing capacity of the glasses.

Finally, the impact of adding MnO to the prepared Mn-glasses on the effective atomic number (Z_{eff}) is studied. The variation of Z_{eff} as a function of photon energy (MeV) and MnO

content for the prepared Mn-glasses is depicts in Figure 11. It is clearly that according to relation (6), the trend of Z_{eff} variation is similar to that of both linear and mass attenuation coefficients (μ and μ_m).

4. Conclusion

The impact of adding MnO to the prepared Mn-glasses with chemical composition $40B_2O_3$+40PbO+(20-x)K_2O+xMnO: x= 0-5 mol% on structure, optical, magnetic and gamma-ray protection properties have been examined. Results revealed the following items:

1- The density of the Mn-glasses was increased from 4.83±0.01 g/cm^3 to 5.23±0.01 g/cm^3 as MnO content increased from 0 to 5 mol%.
2- The obtained direct E_g values were 2.84, 2.59, 2.41, 2.19, 1.95, and 1.84 eV for the Mn-0, Mn-1, Mn-2, Mn-3, Mn-4, and Mn5 glass samples, respectively.
3- The deconvoluted spectra of the investigated samples demonstrate that as the MnO_2 concentration increases in the glass network the intensity and width of the IR bands were increased. As well as a higher degree of disorder occurred when more Mn^{2+} ions access the network and serve as structural modifiers.
4- There is more agreement between the results of FTIR and UV-Vis data.
5- The magnetic measurements showed that the coercivity field (H_c) was improved by increasing MnO substitution ratio.
6- Results of the $\mu_{Mn-glass}$ follows the order: $\mu_{Mn\text{-}0} < \mu_{Mn\text{-}1} < \mu_{Mn\text{-}2} < \mu_{Mn\text{-}3} < \mu_{Mn\text{-}4} < \mu_{Mn\text{-}5}$.
7- HVL rises as μ decreases and vice versa. The range of the HVL is 0.002 – 3.378, 0.002 – 3.334, 0.002 – 3.291, 0.002 – 3.248, 0.002 – 3.176, and 0.002 – 3.106 cm for Mn-0, Mn-1, Mn-2, Mn-3, Mn-4, and Mn-5, respectively.
8- The trend of Z_{eff} variation is similar to that of both linear and mass attenuation coefficients (μ and μ_m).

One can conclude that the prepared Mn-glasses can be used in several optical and radiation protection areas.

References

[1] N.P. Bansal, R.H. Doremus, "Handbook of Glass Properties", Academic Press, 1986.

[2] M.I. Sayyed, Y. Al-Hadeethi, Maha M. AlShammari, Moustafa Ahmed, Saleh H. Al-Heniti, Y.S. Rammah, Physical, optical and gamma radiation shielding competence of newly boro-tellurite based glasses: TeO_2–B_2O_3–ZnO–Li_2O_3–Bi_2O_3, Ceramics International 47 (2021) 611–618.

[3] A.M. Abdelghany, M.A. Ouis, M.A. Azooz, H.A. EllBatal, Defect formation of gamma irradiated MoO_3-doped borophosphate glasses. Spectrochimica Acta Part A: Molecular and Biomolecular Spectroscopy, 114 (2013) 569-574.

[4] H. Wen, P.A. Tanner, Optical properties of 3d transition metal ion doped sodium borosilicate glass, J. Alloys Compd. 625 (2015) 328–335.

[5] A. M. Abdelghany, Y.S. Rammah, Transparent Alumino Lithium Borate Glass-Ceramics: Synthesis, Structure and Gamma-Ray Shielding Attitude, Journal of Inorganic and Organometallic Polymers and Materials 31 (2021) 2560–2568.

[6] Y. Al-Hadeethi, M.I. Sayyed, Bahaaudin M. Raffah, E. Bekyarova, Y.S. Rammah, Optical properties and radiation shielding features of Er^{3+} ions doped B_2O_3–SiO_2–Gd_2O_3–CaO glasses, Ceramics International 47 (2021) 3421–3429.

[7] A.S. Abouhaswa, Gamal M. Turky, Y.S. Rammah, Characterization of zinc lead-borate glasses doped with Fe^{3+}: Optical, dielectric and ac-conductivity investigations, J. Mater. Sci.: Mater. Electron (2020). https://doi.org/10.1007/s10854-020-04262-1.

[8] M. Rashad, Atif Mossad Ali, M.I. Sayyed, H.H. Somaily, H. Algarni, Y.S. Rammah, Radiation attenuation and optical features of lithium borate glasses containing barium: B_2O_3.Li_2O.BaO, Ceramics International 46 (2020) 21000–21007.

[9] Atif Mossad Ali, Y.S. Rammah, M. I. Sayyed, H. H. Somaily, H. Algarni, M. Rashad, The impact of lead oxide on the optical and gamma shielding properties of barium borate glasses. Applied Physics A 126 (2020) 280.

[10] A. Bhogi, P. Kistaiah, Structural and optical properties of CuO doped lithium borate glasses, J. Phy. Chem. Glasses 56 (2015) 197–202.

[11] S.P.H.S. Hashim, H.A.A. Sidek, M.K. Halimah, K.A. Matori, W.M.D.W. Yusof, M.H. M. Zaid, The effect of remelting on the physical properties of borotellurite glass doped with manganese, Int. J. Mol. Sci. 14 (2013) 1022–1030.

[12] T. Satyanarayana, M.A. Valente, G. Nagarjuna, N. Veeraiah, Spectroscopic features of manganese doped tellurite borate glass ceramics, J. Phys. Chem. Solids 74 (2013) 229–235.

[13] A. Terczynska-Madej, K. Cholewa-Kowalska, M. Laczka, The effect of silicate network modifiers on color and electron spectra of transition metal ions, Opt. Mater. 32 (2010) 1456–1462.

[14] P.V. Reddy, C.L. Kanth, V.P. Kumar, N. Veeraiah, P. Kistaiah, Optical and thermoluminescence properties of R_2O-RF-B_2O_3 glass system doped with MnO, J. Non-Cryst. Solids 351 (2005) 3752–3759.

[15] Y.S. Rammah, I.O. Olarinoye, F.I. El-Agawany, A. El-Adawy, El Sayed Yousef, The impact of PbF_2 on the ionizing radiation shielding competence and mechanical properties of TeO_2–PbF_2 glasses and glass-ceramics, *Ceramics International* (2020). https://doi.org/10.1016/j.ceramint.2020.09.100.

[16] Y.S. Rammah, I.O. Olarinoye, F.I. El-Agawany, A. El-Adawy, El Sayed Yousef, The *f*-factor, neutron, gamma radiation and proton shielding competences of glasses with Pb or Pb/Bi heavy elements for nuclear protection applications, *Ceramics International* (2020). https://doi.org/10.1016/j.ceramint.2020.07.197.

[17] Y.S. Rammah, A. Askin, A.S. Abouhaswa, F.I. El-Agawany, M.I. Sayyed, Synthesis, physical, structural and shielding properties of newly developed B2O3 –ZnO–PbO–Fe_2O_3 glasses using Geant4 code and WinXCOM program. Appl. Phys. A 125 (2019) 523.

[18] M.I. Sayyed, I.A. El-Mesady, A.S. Abouhaswa, A. Askin, Y.S. Rammah, Comprehensive study on the structural, optical, physical and gamma photon shielding features of B2O3 –Bi2O 3 –PbO–TiO2 glasses using WinXCOM and Geant4 code. J. Mol. Struct. 1197 (2019) 656–665.

[19] M.I. Sayyed, Y.S. Rammah, A.S. Abouhaswa, H.O. Tekin, B.O. Elbashir, ZnO-B2O3 -PbO glasses: synthesis and radiation shielding characterization. Phys. B. Phys. Condens. Matter 548 (2018) 20–26

[20] H.H. Hegazy, M.S. Al-Buriahi, Faisal Alresheedi, F.I. El-Agawany, Chahkrit Sriwunkum, R. Neffati, Y.S. Rammah, Nuclear shielding properties of B_2O_3–Bi_2O_3–SrO glasses modified with Nd_2O_3: Theoretical and simulation studies, Ceramics International 47 (2021) 2772–2780.

[21] E. Şakar, E., Ö. F. Özpolat, B. Alım, M.I. Sayyed, M. Kurudirek, Phy-X/PSD: development of a user friendly online software for calculation of parameters relevant to radiation shielding and dosimetry, Radiation Physics and Chemistry 166 (2020) 108496.

[22] M. Farouk, A. Samir, F. Metawe, M. Elokr, Optical absorption and structural studies of bismuth borate glasses containing Er^{3+} ions, J. Non-Cryst. Solids 371–372 (2013) 14–21.

[23] M. Bosca, L. Pop, G. Borodi, P. Pascuta, E. Culea, XRD and FTIR structural investigations of erbium-doped bismuth-lead-silver glasses and glass ceramics, J. Alloy. Comp., 479 (2009 579-582

[24] S. Gu, Z. Wang, S. Jiang, H. Lin, Influences of Fe_2O_3 on the structure and properties of Bi_2O_3-B_2O_3-SiO_2 low-melting glasses, Ceram. Int., 40 (2014),7643-7645

[25] M. Pal, B. Roy, M. Pal, Structural characterization of borate glasses containing zinc and manganese oxides. J. Mod. Phys. **2**(9) (2011) 1062.

[26] C. Gautam, A.K. Yadav, A.K. Singh, A review on infrared spectroscopy of borate glasses with effects of different additives. ISRN Ceram. **2012**, 17 (2012)

[27] P.V. Rao, G.N. Raju, P.S. Prasad, C. Laxmikanth, N. Veeraiah, Transport and spectroscopic properties of nickel ions in ZnO-B_2O_3-P_2O_5 glass system, Opt. - Int. J. Light Electron Opt. (2015) 54–57.

[28] J. Tauc, A. Menth, States in the gap, J. Non-Cryst. Solids 8–10 (1972) 569.

[29] M.S. Sadeq, H.Y. Morshidy, Effect of samarium oxide on structural, optical and electrical properties of some alumino-borate glasses with constant copper chloride, J. Rare Earths, 38 (2020) 770-775.

[30] A.A. El-Daly, M.A. Abdo, H.A. Bakr, M.S. Sadeq, Impact of cobalt ions on the phonon energy and ligand field parameters of some borate glasses, J. Non-Cryst. Solids, 555 (2021) 120535.

[31] A. Samir, M.A. Hassan, A. Abokhadra, L.I. Soliman, M. Elokr, Characterization of borate glasses doped with copper oxide for optical application, Opt. Quantum Electron. 51 (2019) 123.

[32] A. Okasha, S.Y. Marzouk, A.M. Abdelghany, Design a tunable glasses optical filters using CuO doped fluoroborate glasses, Opt. Laser Technol. 137 (2021) 106829.

Figures

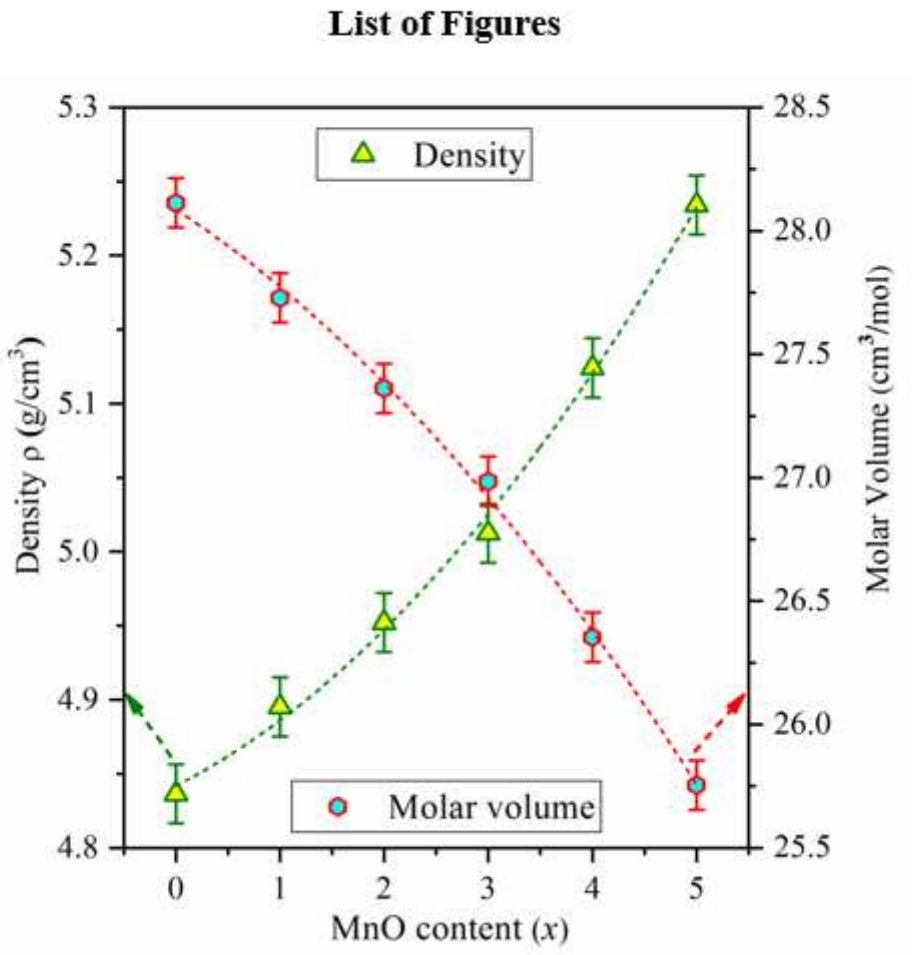

Figure 1

Density and molar volumeas a function of MnO content of $40B_2O_3$+40PbO+(20-x)K_2O+xMnO: x=0, 1, 2, 3, 4, and 5 mol%

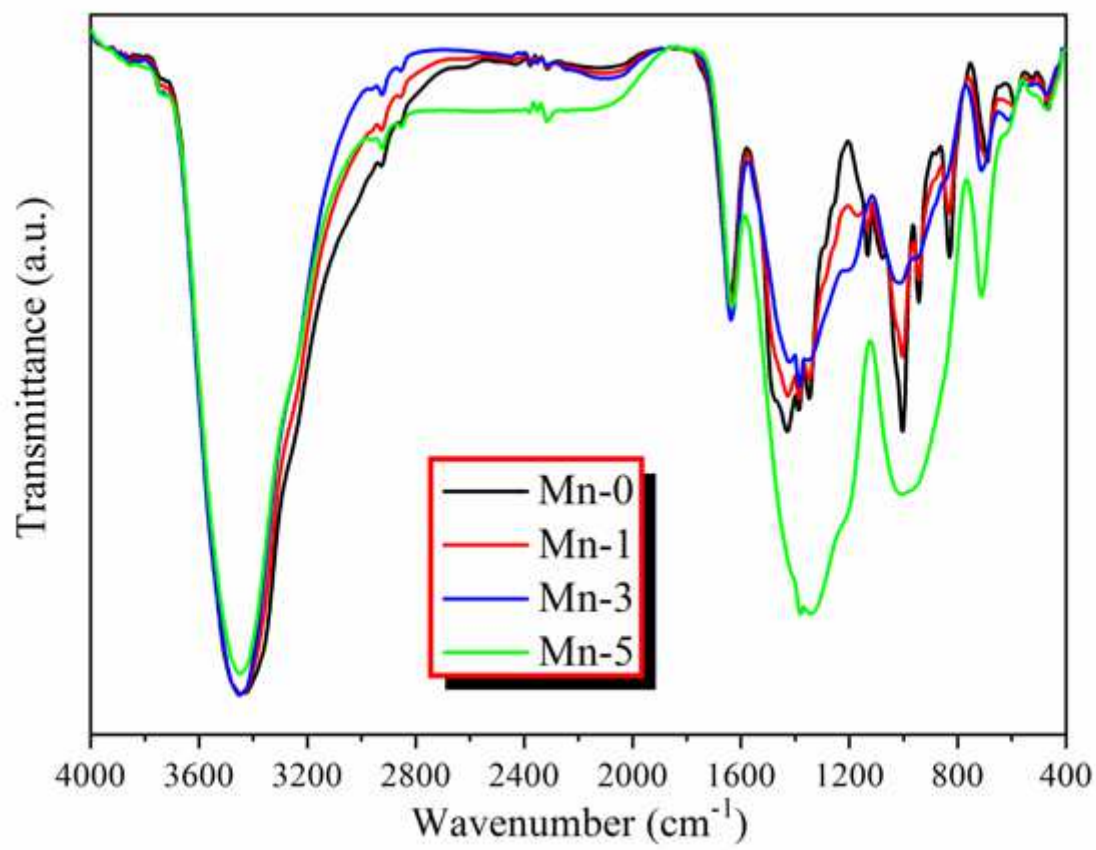

Figure 2

FTIR spectra of the fabricated glass samples with the composition $40B_2O_3+40PbO+(20-x)K_2O+xMnO$ (x=0, 1, 3, and 5 mol%).

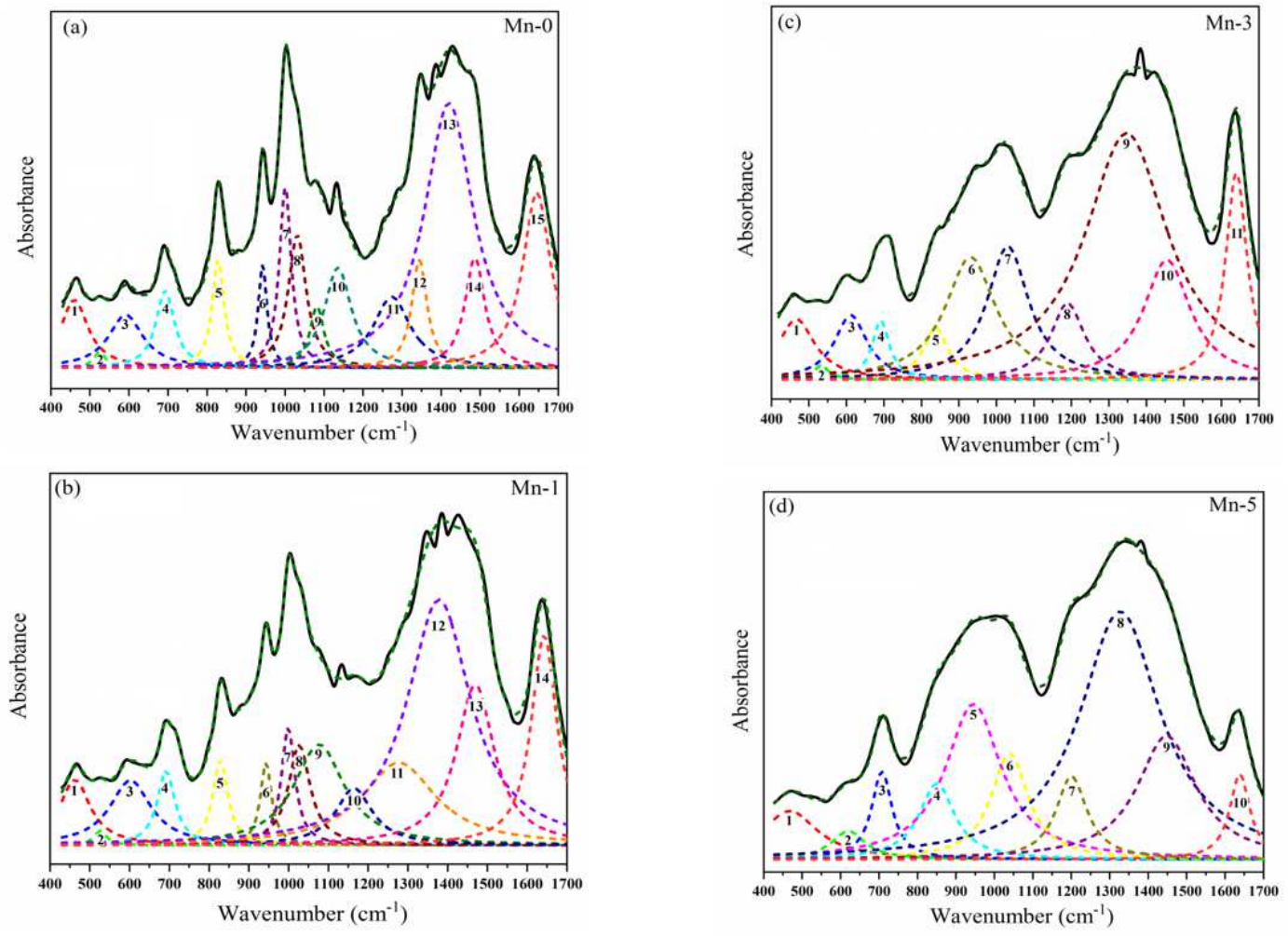

Figure 3

FTIR-deconvoluted spectra of the samples (a) Mn-0, (b) Mn-1, (c) Mn-3, and (d) Mn-

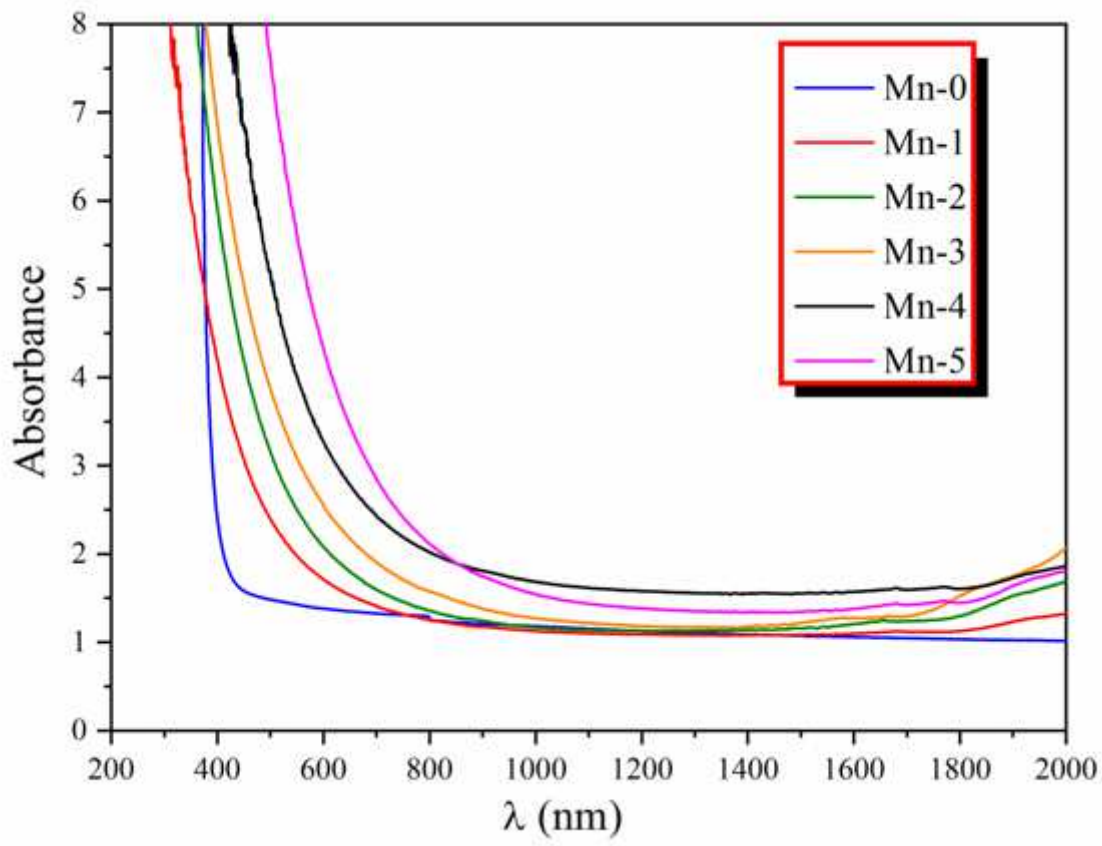

Figure 4

Absorbance spectra of the prepared Mn-glasses.

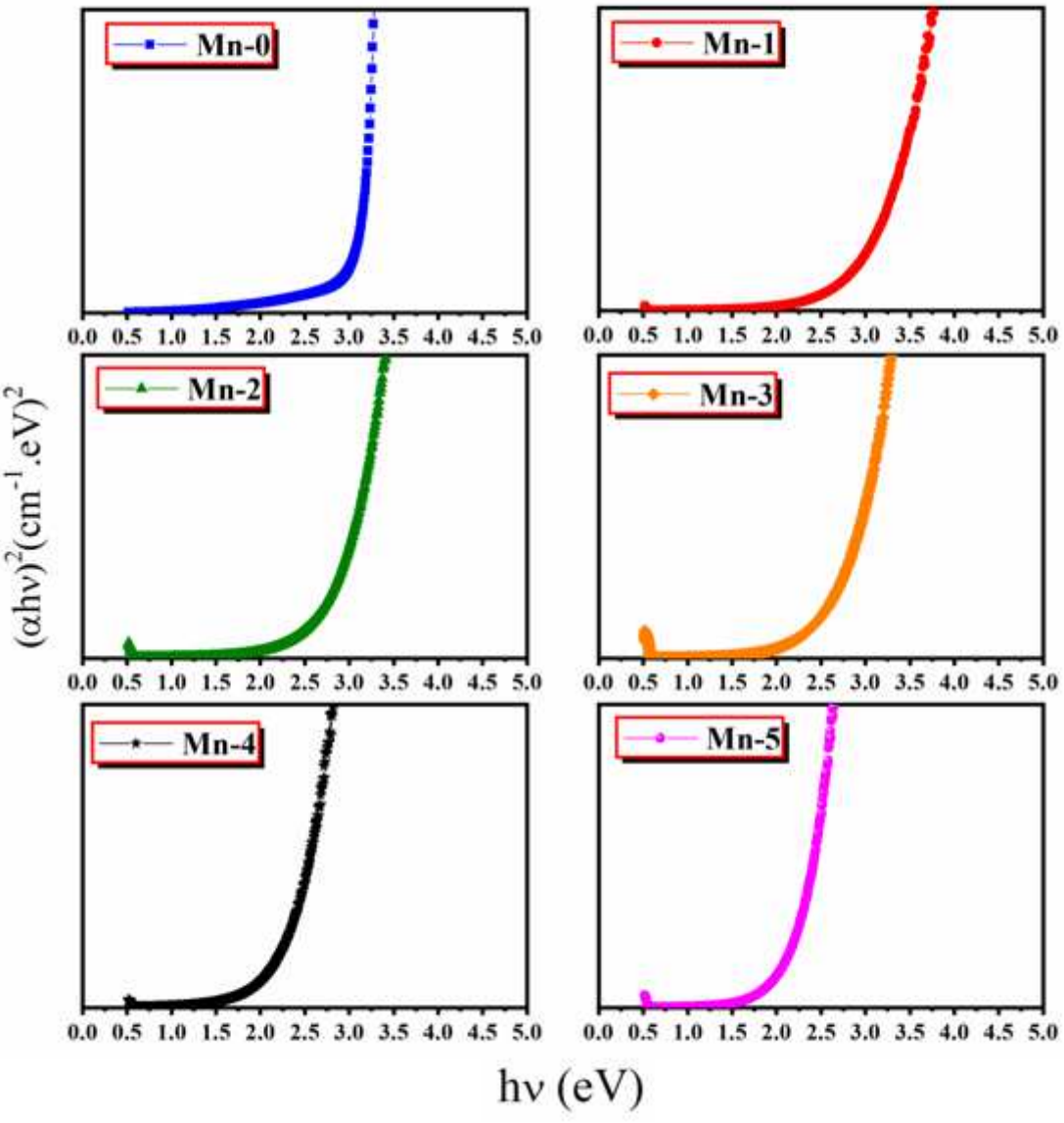

Figure 5

Variation of $(\alpha h\nu)^2$ with (hν) of the prepared Mn-glasses.

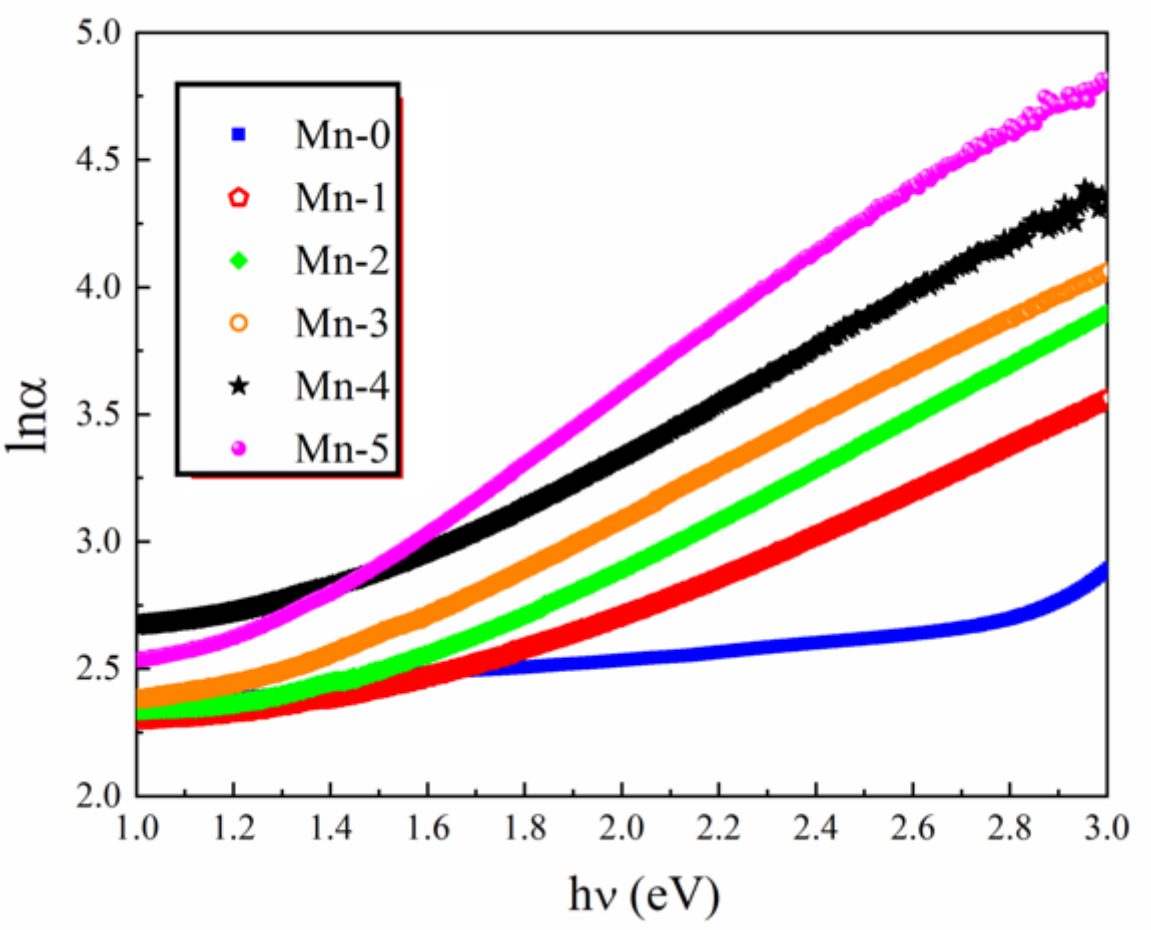

Figure 6

Variation of (lnα) with (hν) of the prepared Mn-glasses.

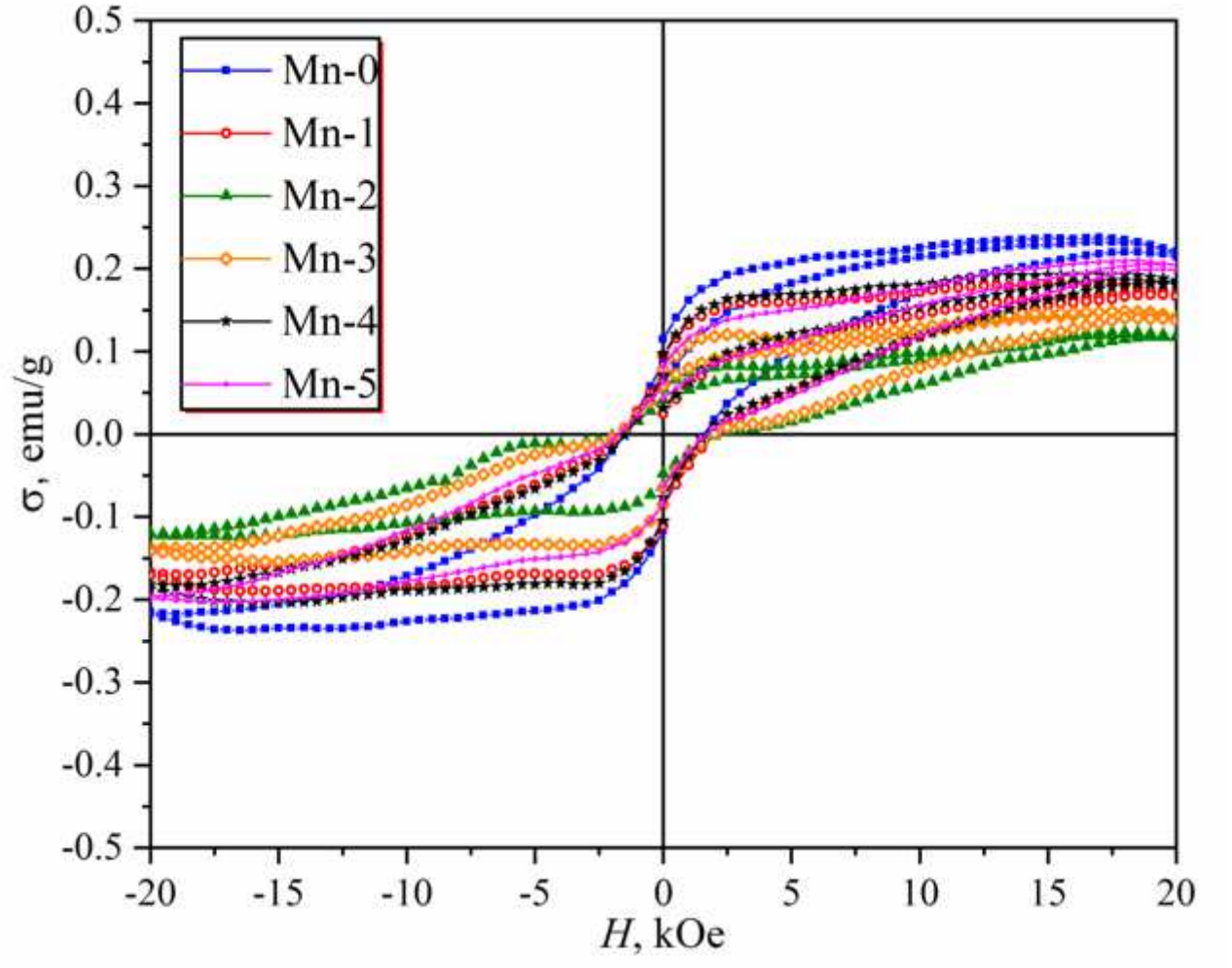

Figure 7

Room temperature hysteresis loops for the prepared glass samples.

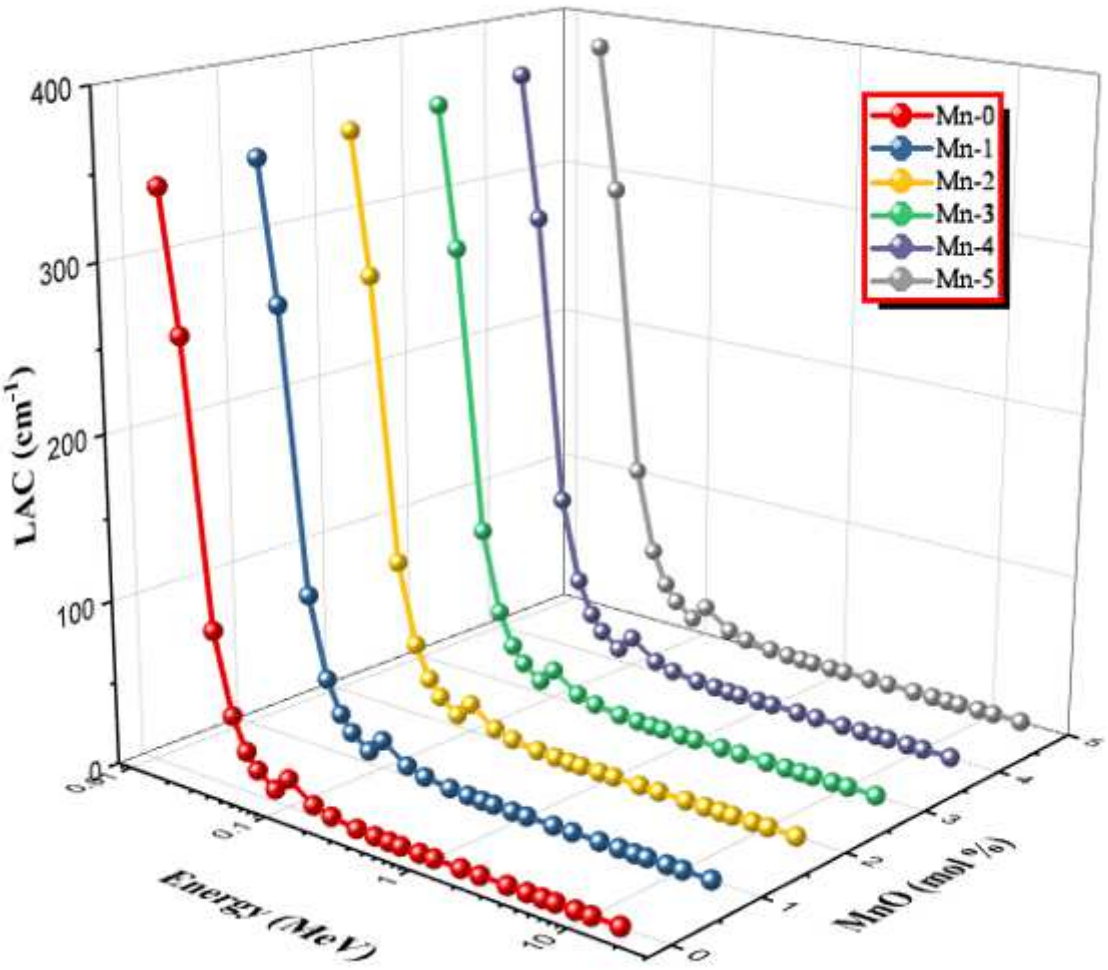

Figure 8

LAC as a function of photon energy (MeV) and MnO content for the prepared Mn-glasses.

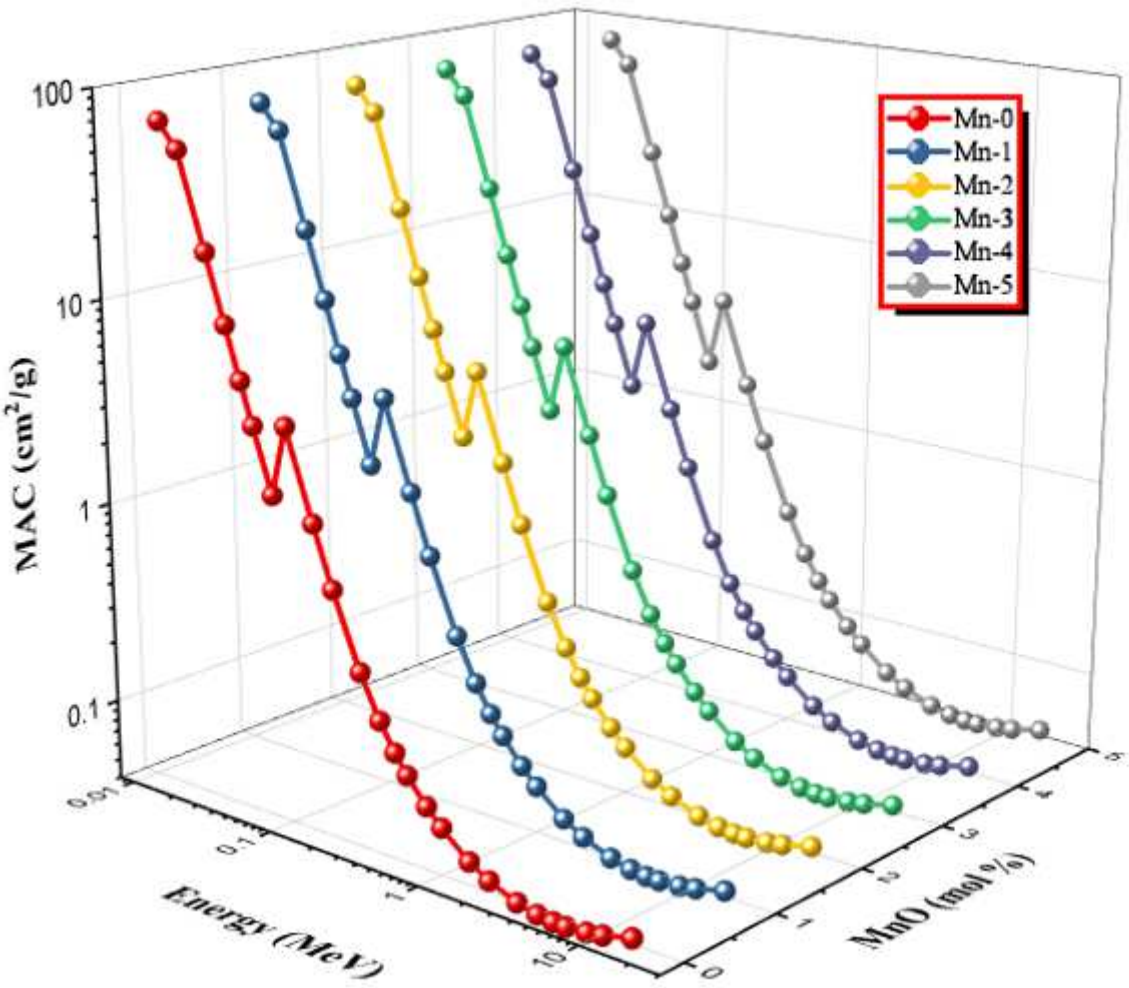

Figure 9

MAC as a function of photon energy (MeV) and MnO content for the prepared Mn-glasses.

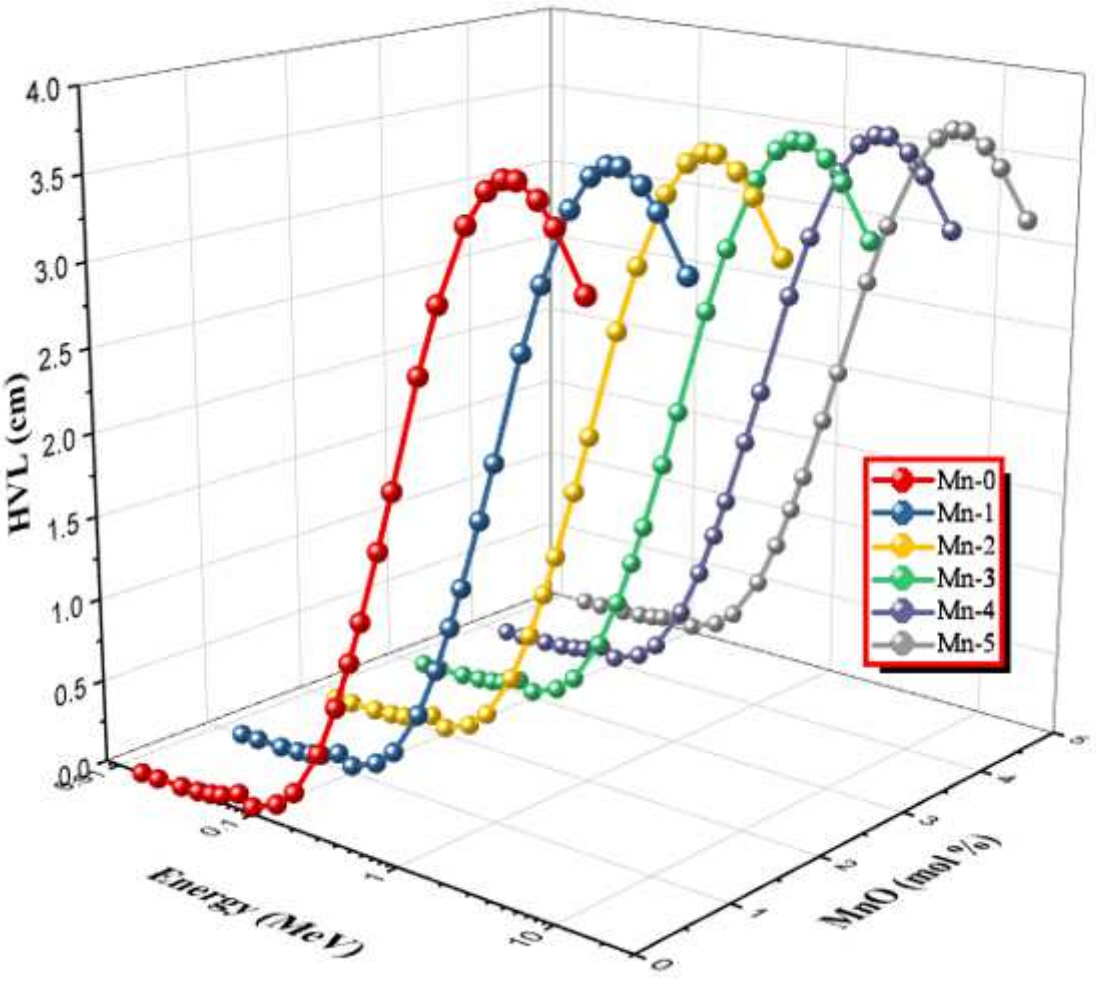

Figure 10

HVL as a function of photon energy (MeV) and MnO content for the prepared Mn-glasses.

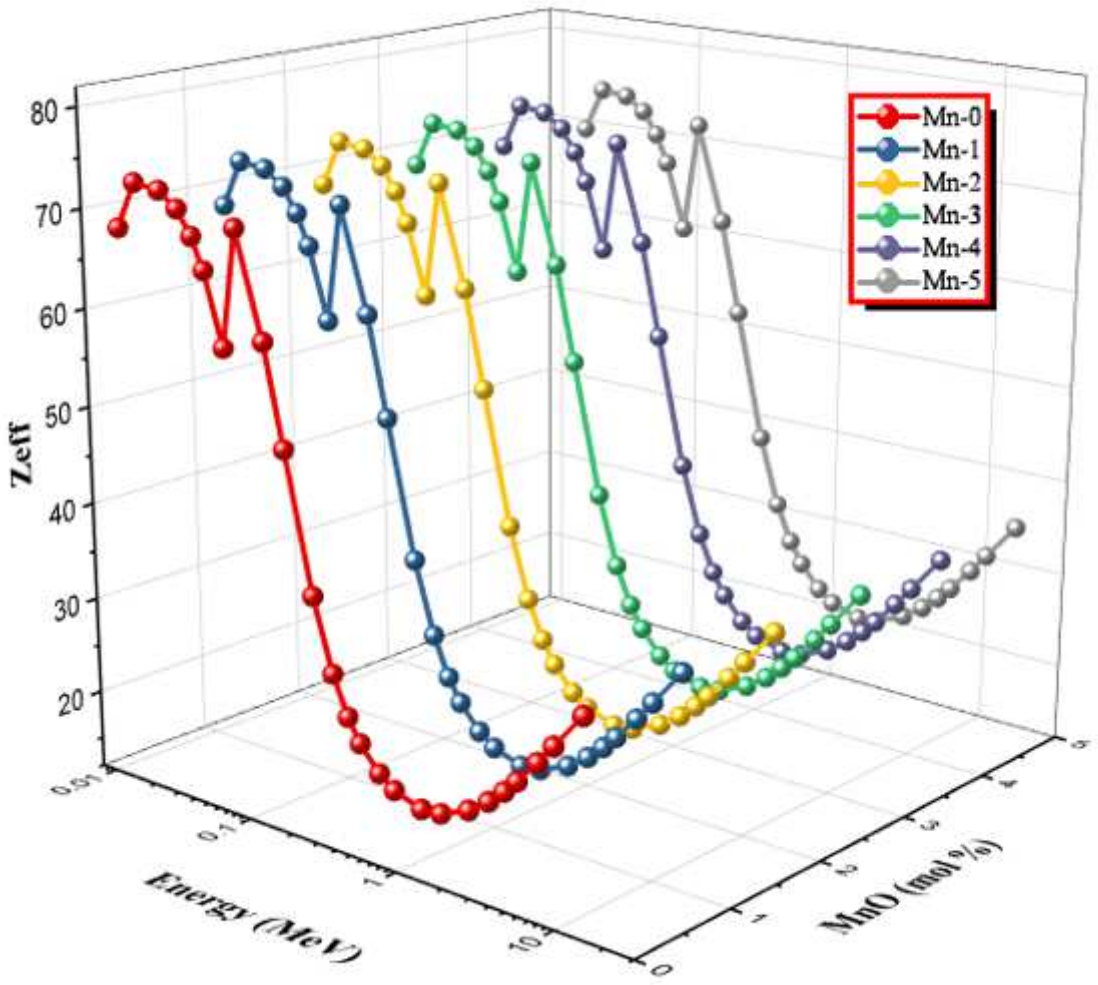

Figure 11

Z_{eff} as a function of photon energy (MeV) and MnO content for the prepared Mn-glasses.